The Cerebellum (2024) 23:471–478
https://doi.org/10.1007/s12311-023-01556-y

ORIGINAL ARTICLE

Reduction of Microvessel Number and Length in the Cerebellum of Purkinje Cell Degeneration Mice

Yaroslav Kolinko[1,2] · **Milena Kralickova**[1,2] · **Jan Cendelin**[1,3]

Accepted: 5 April 2023 / Published online: 18 April 2023

Abstract

Degenerative effects of nerve tissuesare often accompanied by changes in vascularization. In this regard, knowledge about hereditary cerebellar degeneration is limited. In this study, we compared the vascularity of the individual cerebellar components of 3-month-old wild-type mice ($n=8$) and Purkinje cell degeneration (pcd) mutant mice, which represent a model of hereditary cerebellar degeneration ($n=8$). Systematic random samples of tissue sections were processed, and laminin was immunostained to visualize microvessels. A computer-assisted stereology system was used to quantify microvessel parameters including total number, total length, and associated densities in cerebellar layers. Our results in pcd mice revealed a 45% ($p<0.01$) reduction in the total volume of the cerebellum, a 28% ($p<0.05$) reduction in the total number of vessels and a lower total length, approaching 50% ($p<0.001$), compared to the control mice. In pcd mutants, cerebellar degeneration is accompanied by significant reduction in the microvascular network that is proportional to the cerebellar volume reduction therefore does not change density of in the cerebellar gray matter of pcd mice.

Keywords Microvessels · Capillary · Stereology · Ataxia · Cerebellar degeneration · Pcd mouse

Introduction

Neurodegenerative diseases are characterized by progressive extinction of certain populations of neurons. Loss of neurons together with their functional impairments preceding cell death is responsible for most neurological manifestations. Nevertheless, such diseases can be accompanied by other changes in the brain tissue modifying its local niche. This may consequently influence regenerative capacity and neural plasticity level and thereby have an impact on therapeutic possibilities. These changes may include modified density or activity of glial cells [1, 2], abnormal levels of trophic factors or other information molecules, inflammatory mediators [3–6], and changed microvasculature.

Abnormal capillary density or a changed character of the capillary bed and abnormal angiogenesis have been found in some neurodegenerative diseases [7–9]. Vasculature of the tissue is necessary for oxygen and nutrient delivery and the disposal of metabolic waste products but is also a source for various mediators and cells of the immune system. Thus, the microvascular bed is crucial for tissue functioning and trophic state, tissue damage healing and inflammation and delivery or clearing of signaling molecules involved in control of cell death/survival with both positive and negative effects. Vascular bed density may also affect graft survival or rejection processes [10].

Therefore, recognizing microvascular bed changes in tissue injured by a neurodegenerative process might help to explain some specific features of the disease, or phenomena of problematic recovery and insufficient effect of therapy. Understanding general principles of how local tissue niches, including microvascular bed changes, influence tissue, and function recovery and neural plasticity might substantially help to predict the efficiency of certain therapeutic approaches in neurodegenerative diseases accompanied by particular neuropathologies.

There are many types of hereditary cerebellar degeneration that have detrimental impacts on complex cerebellar functions.

✉ Yaroslav Kolinko
Yaroslav.Kolinko@lfp.cuni.cz

[1] Biomedical Center in Pilsen, Faculty of Medicine in Pilsen, Charles University, Pilsen, Czech Republic

[2] Department of Histology and Embryology, Faculty of Medicine in Pilsen, Charles University, Pilsen, Czech Republic

[3] Department of Pathophysiology, Faculty of Medicine in Pilsen, Charles University, Pilsen, Czech Republic

Since there is no truly efficient therapy allowing suppression of the cerebellar degeneration progress in most of these diseases, they lead to progressive motor and cognitive-affective cerebellar syndromes and severe disability for the patient [11]. To investigate pathogenesis and therapeutic methods, various cerebellar mutant mouse strains have been used. These strains reflect a spectrum of human hereditary cerebellar degenerations and allow searching for differences between diseases and disease-specific features [12, 13].

In our previous study, we showed that in Lurcher mutant mice, cerebellar degeneration, and cerebellar volume reduction are accompanied by decreased absolute quantities of capillaries, while relative microvessel densities are increased [14]. Contrary to wild-type mice, cerebellar grafts showed a poor tendency to integrate within the host cerebellar tissue in Lurcher mutant mice [15–17]. Similar differences were not observed in Purkinje cell degeneration (pcd) mutant mice [17]. Since abnormal microvasculature could be one of the factors determining graft development, analysis of the capillary bed in pcd mice would be of interest.

Pcd mice are one of the most frequently used cerebellar mutant mice. They are homozygous for Agtpbp1^{pcd}/J mutations in the gene encoding cytosolic ATP/GTP binding protein 1 (synonyms: cytosolic carboxypeptidase-like protein, CCP1, Nna1), which is intensively expressed in cerebellar Purkinje cells, olfactory bulb mitral cells, and retinal photoreceptors [18]. The effect of the mutation is a rapid and almost complete degeneration of Purkinje cells by apoptotic [19] or autophagic [20] mechanisms. The degeneration starts at postnatal day 20 [21], and by postnatal day 28, it is nearly complete in most parts of the cerebellum [22]. The degeneration of cerebellar granule cells is secondary to the loss of Purkinje neurons and is exponentially progressive [23, 24]. Cerebellar nuclei are only slightly reduced in size [25]. Inferior olivary neurons start to disappear between postnatal days 17 and 23, and by postnatal day 300, the reduction has reached 49% [23]. Pcd mice also suffer from slow, progressive degeneration of the retina and olfactory bulb mitral cells [22, 26–28] and degenerative changes in the thalamus [29].

The aim of this study was to provide a quantitative analysis of the microvascular bed in the cerebella of adult pcd mice based on stereology techniques for the detection of potential differences in microvascularization. For this purpose, their cerebella were compared with healthy strain- and age-matched controls showing a normal state of microvasculature.

Materials and Methods

Animals and Ethical Statements

Three month old (± 1 week) B6.BR-Agtpbp1^{pcd}/J strain pcd mice with clinical signs of cerebellar ataxia (four males, four females) and strain-matched wild-type (WT, clinically healthy individuals, i.e., mutation noncarriers or heterozygotes) mice (four males, four females) were used. The mice were kept under standard conditions in a temperature- and humidity-controlled room (22–24 °C; 30–60%) with a 12/12 h light/dark cycle (6 am–6 pm). Food (commercial pellet diet) and water were available ad libitum.

The experiments reported here were conducted in full compliance with the European Union guidelines for scientific experimentation on animals and with the permission of the Ethical Commission of the Faculty of Medicine in Pilsen. All efforts were made to minimize suffering.

Tissue Processing

The mice were euthanized by cervical dislocation. Their brains were removed and fixed in 10% phosphate buffered formalin at 4 °C for 30 days until embedding in paraffin blocks. Each block was sectioned into 18-µm thick serial Sects. (120 ± 57 sections per brain) using a Leica RM 2145 microtome (Germany). Every 30th horizontal section was mounted on glass slides, immunostained using the polyclonal rabbit anti-laminin antibody (dilution 1:1000; Dako, Glostrup, Denmark, No. Z009701), colorized with diaminobenzidin (Dako, DAB Chromogen), and counterstained with hematoxylin. In this work, we used the same immunohistochemistry protocols as in previous projects [14, 30]. This sampling design generated 3 to 8 systematic-uniform sections that were collected depending on the tissue block thickness of the cerebellum.

Quantitative Histological Analysis

Stereological analyses of sections for each mouse cerebellum were done blind to genotype. The most current version of Stereologer software (v11.0) (SRC Biosciences, Tampa, FL, USA) running on a PC equipped with a Nikon Eclipse Ti-U microscope equipped with standard optical lenses, a high-resolution digital imaging camera (Promicra 3-3CC) and a ProScan III motorized 3-axis step motor (Prior Electronics, UK), were used for the analyses. The combination of these devices allows the automatic selection of the series of equidistant fields of view and to project related probe frames there. This way, the most statistically efficient selection of samples through the entire cerebellum, as the region of interest, was carried out. As shown in Supplement 1, stereology data were collected for total region volume (V), total number of microvascular segments (total N_{cap}), and total number of microvascular endpoints for the selected cell layers: molecular layer (ML); the layer of granular cells (GL); white matter (WM); and nuclei (N). The Purkinje cell layer was excluded from the analysis because its blood supply is provided by the capillaries of adjacent layers [14, 31].

The total regional volumes of cell layers were estimated using the Cavalieri principle [32, 33] with a 4 × objective (Plan Fluor, Na 0.13). Estimation of capillary numbers (endpoints) and lengths was performed using a 60 × oil objective (CFI, Plan Apo Lambda, Na 1.4) using excluded 1-µm guard zones at the top and bottom surfaces of each section. The total number of microvascular endpoints was estimated using an optical disector [34] by counting saddle points of capillary branch nodes + 1 (Fig. 1c) [35]. The total N_{cap} is double (2 ×) the number of nodes [33, 35, 36]. Estimates of total L_{cap} were made using the Space Balls probe [33, 37] by double the number of intersections between the central axes of capillaries and the surface of the spherical probes with a standardized diameter (Fig. 1d). The measurements of the diameters of at least one hundred microvessels in each of the layers per case were made in the set of calibrated images (summary see Supplement 2) using OlyVIA 3.4 freeware. The average densities of capillary segments (N_{Vcap}) and/or length density (L_{Vcap}) were calculated as total N_{cap} or total L_{cap} divided by the total volume. Finally, the potential diffusion distance of capillaries was determined in postprocessing using the approach described in [14, 38]. The coefficient of error (CE), a measure of sampling error, was estimated [39], and sampling continued to CE ~ 0.10 across both hemispheres.

Statistical Analysis

Nonparametric methods in Statistica 13 (StatSoft, Inc., Tulsa, OK, USA) were used for statistical analyses of microcirculatory parameters. First, the Mann–Whitney *U* test was performed to test for group effects (WT vs. pcd). Within-group effects were assessed using Friedman ANOVA and Kendall's coefficient of concordance (F_{ANOVA}). Data are presented as the mean ± SD. $P < 0.05$ was considered statistically significant.

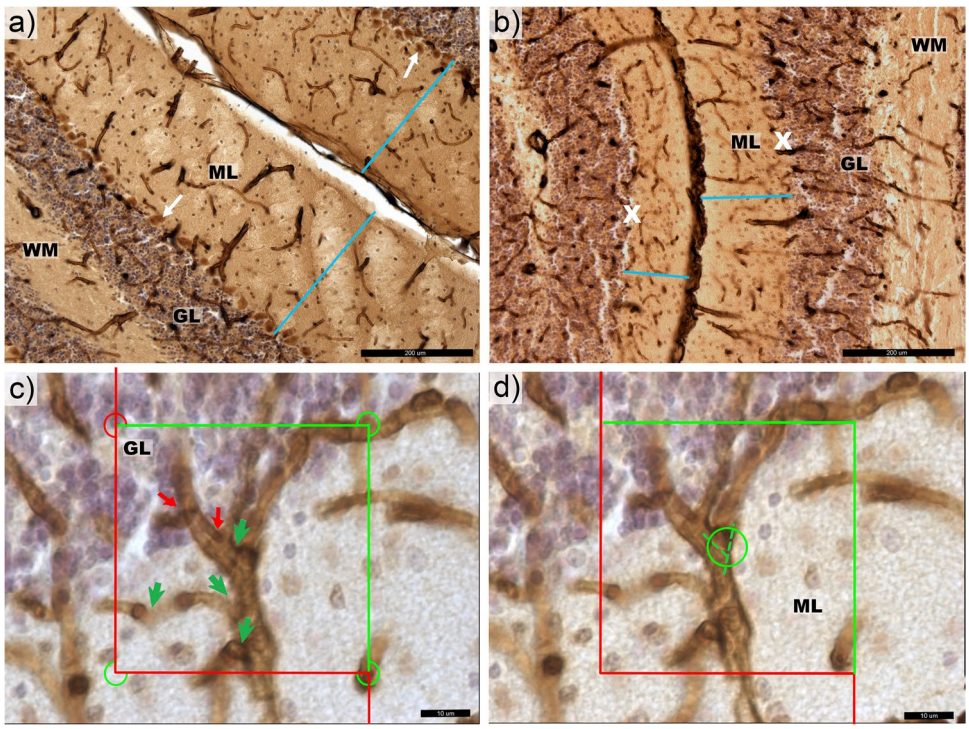

Fig. 1 Microphotograph of the anti-laminin antibody-labeled cerebellar microvessels in control and pcd mice. In contrast to control mice (**a**), the molecular layer (ML) and granular layer (GL) of pcd mice (**b**) showed signs of degeneration associated with the absence of Purkinje cells (white arrows and × show Purkinje cells or place where they are absent in a wild type and a pcd mouse respectively). The thicknesses of ML is shown in blue lines. White matter (WM) seems to be histologically intact. The MLs of pcd mice usually contained capillaries (dark brown) that are thinner than those of wild-type mice. The optical disector frame (**c**) was used for quantifications of "capillary saddle points" (green arrows for ML and red arrows for GL) at branch-points or nodes. Labels for the frame corners were used to distinguish the respective regions of interest (red and green circles) during the analysis. The capillary length was found using the space balls method (**d**) by counting the number of intersections between the surface of the spherical probe and a spline through the center of each capillary (green dotted line). Space bars: a; b–500 µm; c; d–10 µm

Results

With regard to between-group comparisons, stereology studies revealed a 45% reduction in total V in the cerebellum of pcd mice compared to the controls (Mann–Whitney U, $p < 0.01$; (Fig. 2a), which occurs due to changes in the volume of all layers of the cerebellum. First, there was a 60% reduction in the total V of ML (Mann–Whitney U, $p < 0.001$; (Fig. 2b). Second, there was an 87% reduction in the total V of Purkinje cell bodies in the cerebellum of pcd mice compared to the controls (Mann–Whitney U, $p < 0.001$; see supplementary material). These data also demonstrate that the Purkinje cell/ML volume ratio in pcd mice is only 34% of the corresponding ratio in healthy mice (0.029 ± 0.022 for pcd and 0.081 ± 0.036 for WT; see supplement 1). Third, there was a 31% reduction in the total volume of GL (Mann–Whitney U, $p < 0.05$), and a 39% reduction in the total V of WM (Mann–Whitney U, $p < 0.002$). Finally, a solid trend for the reduction in total V of N (Mann–Whitney U, $p = 0.054$) was found.

With the reduction in cerebellar volume, the total N_{cap} was also reduced by 28% in pcd mice (Mann–Whitney U, $p < 0.05$; (Fig. 2d). Moreover, the fraction of small capillaries (≤ 5 µm in diameter) in pcd mice was significantly increased to 90% (Mann–Whitney U, $p < 0.01$), in contrast to healthy mice with 83% of small capillaries in the ML (see Fig. 1a, b and Fig. 2c). At the same time, the fraction of the microvessels with small diameters in the white matter decreases from 66% in healthy mice to 53% in pcd mice (Mann–Whitney U, $p < 0.01$). This was accompanied by a significant increase in the fraction of the microvessels with diameters from 5 to 10 µm here (Mann–Whitney U, $p < 0.01$).

More specifically, stereological studies in pcd mice showed a significant reduction in total N_{cap} in ML from $11{,}5474 \pm 29{,}800$ in control mice to $61{,}558 \pm 23{,}260$ in pcd mice (Mann–Whitney U, $p < 0.05$) and in the nuclei from $18{,}600 \pm 4500$ to $12{,}550 \pm 2300$ in pcd mice (Mann–Whitney U, $p < 0.05$), as shown in Fig. 2e and in the supplement 1. On the other hand, the total N_{cap} was not changed in GL and MW (Fig. 2e).

Our studies found a reduction in the total L_{cap} in pcd mice approaching 50% (Mann–Whitney, $p < 0.001$; Fig. 2g). The largest decrease in the total L_{cap} of 64% relative to WT mice was observed in the ML of pcd mice (Mann–Whitney U, $p < 0.001$). Moreover, the reduction in the *T*otal L_{cap} was more expressed in the ML of pcd males than in pcd females (see Supplement 1). Nevertheless, there was also a significant decrease in GL and N (Mann–Whitney U, $p < 0.01$). Only in the WM were no significant differences in total L_{cap} found (Fig. 2h).

As a result, only the WM was reduced in volume, but without significant changes in total capillary number and length, exhibiting a significant decrease in potential diffusion distance ($p < 0.05$) and an increase in both L_{Vcap} ($p < 0.05$; Fig. 2i) and N_{Vcap} ($p < 0.05$; Fig. 2f).

The comparison between males and females showed twice-lower total L_{cap} in WM of WT females than in WT males (Mann–Whitney U, $p < 0.05$; Supplement 1, rows 35 and Supplement 3). Otherwise, no significant intersex difference was found in any other parameter. There were significant within-group differences (F_{ANOVA} $p < 0.05$; Fig. 2) in all of the estimated vasculature parameters between individual cerebellar structures (ML; GL; WN; and N). For more detailed data, including separate presentations for males and females, see the supplementary material.

Discussion

The pcd mice are a model of neurodegeneration, which results in the death of specific neuronal populations in different regions of the brain with a well-defined time course [22, 40]. The organizational principles of the microcirculatory network in the pcd mouse cerebellum are similar to those described previously [14, 31, 41]. Briefly, the vessels form a dense network in the cerebellar cortex and nuclei. The bodies of Purkinje neurons receive their support from capillaries located predominantly in GL, while their dendrites are supported via the capillaries located in ML. The white matter has almost twice-lower the number density of capillaries compared to the gray matter in the healthy mouse cerebellum (Fig. 2f, i).

Our results demonstrated a significant reduction in the total volume of ML due to primary Purkinje neuron disruption combined with the secondary reduction of GL and WM volumes (Fig. 2a) described earlier [18, 21, 24]. The stereology-based analysis showed a slight insignificant reduction in the total cerebellar nuclei volume in contrast to previously described findings [23, 24]. Here, we demonstrated a reduction in cerebellar volume accompanied by nearly proportional changes in the microvascular network (Fig. 2e, h) as a component of the neuropathology in *pcd* mutant mice. Consequently, these mutants show reduced absolute quantities of capillaries but almost normal microvessel densities at the age of 3 months. Thus, diffusion distance, one of the factors crucial for the maintenance of extracellular homeostasis, remains comparable to that in healthy cerebella.

At this moment, we cannot identify whether the smaller absolute quantities of the capillaries are due to less intensive angiogenesis in the developing cerebellum in which a rapid neurodegeneration simultaneously proceeds [42], or due to secondary reduction of capillaries that have already been developed [41]. Neurodegeneration has a relatively early onset and fast progression in pcd mice. Therefore, it

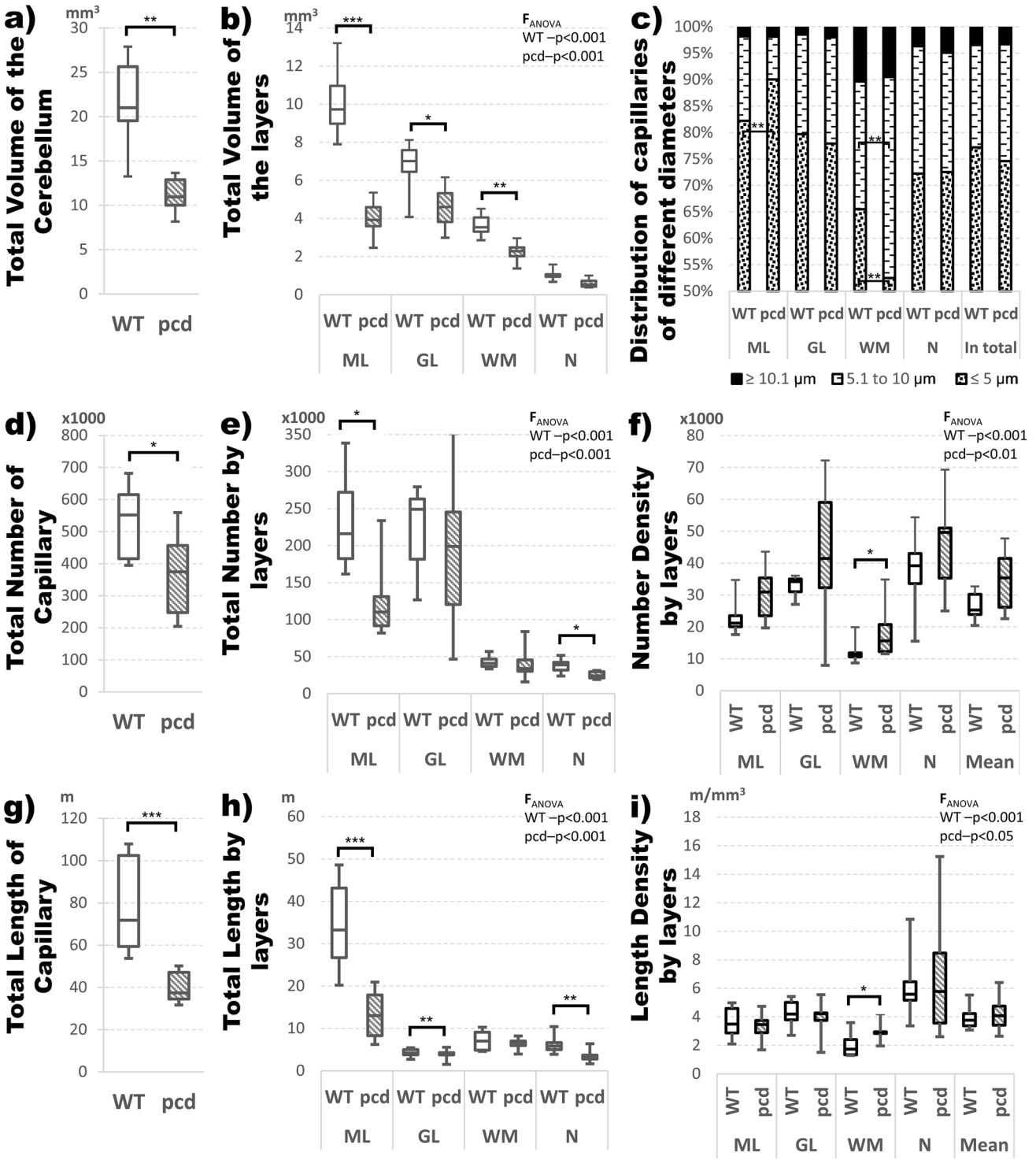

Fig. 2 Comparing quantitative parameters of the microvascular bed of entire cerebellum and it histological compartments in wild-type mice (WT) and pcd mice. ML — labeled molecular layer; GL — granular layer; WM — white matter; N — nuclei. The box-and-whisker plots present quartiles, and the medians are represented by the lines between the first and second quartiles. The significance of within-group comparisons (F_{ANOVA}) between cerebellar layers (ML; GL; WM; and N) for each group is presented in the top right corner of a single diagram. The corresponding parameters of the between-group effect were compared using the Mann–Whitney *U* test: $*p<0.05$; $**p<0.01$; $***p<0.001$

could interfere with late stages of cerebellar development, including the generation of new capillaries in the growing tissue. The combination of both mechanisms is indeed also possible. To answer this question, a more detailed study of different ontogenetic stages in pcd mice would be necessary.

The fraction of the capillaries with ≤ 5 µm in diameter was increased in the molecular layer and decreased in the white matter of the *pcd* cerebellum (Fig. 2c). Furthermore, there are single capillaries with thin hair-like twisted lumens (Fig. 1a, b). However, this effect to some extent may be induced by differences in tissue shrinkage during histological processes due to differences in the molecular structure of the tissue [19, 40].

Microvascular bed features are different from those we have found previously in Lurcher mutant mice [14]. First, it is important to mention that in Lurcher mice cerebellar volume reduction is more severe than in pcd mice (~ 71% in Lurcher opposed to ~ 43% in pcd mice). Second, the absolute number of capillaries is lower, but not proportional to cerebellar volume reduction, in Lurcher mice in contrast to pcd mice (for ~ 53% reduction in Lurcher instead to ~ 40% in pcd mice). Thus, capillary densities almost doubled in Lurcher mice but remained almost unchanged in the cerebellar gray matter of the pcd mice (Fig. 2f, i). Furthermore, the average length of the capillaries remained unchanged in pcd mice. Purkinje cell degeneration appears at approximately postnatal days 8–10, and degeneration of granule cells is more dramatic in Lurcher mice [43], which could explain the more significant volume reduction and, consequently, a secondary increase in relative capillary densities. Thus, these differences in neuronal degeneration course could potentially be responsible for different changes in the microvascular bed in the cerebellum.

As mentioned above, cerebellar embryonic grafts exhibit a poor tendency to become integrated into the host cerebellum in Lurcher mice [15–17]. Increased capillary density and shorter diffusion distance could increase exposure of the graft to pro-inflammatory cytokines [6, 44] and be hypothetically one of the factors limiting migration of grafted cells and axon sprouting into the host tissue [14]. These present findings are in line with this hypothesis since in pcd mice having nearly normal capillary densities and diffusion distances in the cerebellum, the grafts are integrated as well as in the healthy cerebellum [17].

We believe that the data obtained in this work provide a basis for further research. For example, related vascular changes could arise at the different stages of degeneration and restrict structural development in certain regions of the entire brain. However, both the age- and location-related directions require their own unique sampling approach depending on the chosen objective. The study of the angiogenesis factors can also become an independent followed research direction in this area.

Conclusion

In conclusion, we confirm the reduction in the volume of the pcd mutant cerebellum, particularly its granule and molecular layers [40], using unbiased and efficient stereological methods. Reduction of the white matter can be explained by the extinction of Purkinje cell axons and the reduction of climbing fibers [43].

Cerebellar degeneration was accompanied by significant changes in the microvascular network in pcd mutants. However, the reduction of the capillary number and length does not affect their density in the cerebellar gray matter of *pcd* mice, in contrast to the Lurcher mutants [14]. This suggests, reduction of vascular bed is proportional to cerebellar tissue loss. The question remains whether it is due to abnormal angiogenesis due to changed signaling in the niche of early onset neurodegeneration or a secondary and subsequent extinction of the capillaries in response to the existing neurodegeneration. Anyway, proportionality of reduction of both the capillaries and neural tissue suggest that vascular changes are more severe specifically in structures with advanced degeneration.

Supplementary Information The online version contains supplementary material available at https://doi.org/10.1007/s12311-023-01556-y.

Author Contribution Dr. Kolinko performed the histological morphometry, the data analysis, and the literature search and wrote the manuscript. Dr. Cendelin was responsible for the mouse brain collections and provided support during the literature search and writing of the manuscript. All the authors contributed equally to the generation of ideas, general editing, and revising the text critically for important intellectual contention. The final manuscript preparation was conducted by the first author.

Funding This work was supported by the Cooperatio Program, research area MED/DIAG.

Data Availability The authors confirm that the data supporting the findings of this study are available within the article and its supplementary materials.

Declarations

Conflict of Interest The authors declare no competing interests.

References

1. Qu W, Johnson A, Kim JH, Lukowicz A, Svedberg D, Cvetanovic M. Inhibition of colony-stimulating factor 1 receptor early in disease ameliorates motor deficits in SCA1 mice. J Neuroinflamm. 2017;14:107. https://doi.org/10.1186/s12974-017-0880-z.
2. Gyengesi E, Liang HZ, Millington C, Sonego S, Sirijovski D, Gunawardena D, et al. Investigation into the effects of tenilsetam on markers of neuroinflammation in GFAP-IL6 mice. Pharm Res. 2018;35:15. https://doi.org/10.1007/s11095-017-2326-9.
3. Wachter C, Eiden LE, Naumann N, Depboylu C, Weihe E. Loss of cerebellar neurons in the progression of lentiviral disease: effects of CNS-permeant antiretroviral therapy. J Neuroinflamm. 2016;13:13. https://doi.org/10.1186/s12974-016-0726-0.

4. Castrogiovanni P, Sanfilippo C, Imbesi R, Maugeri G, Lo Furno D, Tibullo D, et al. Brain CHID1 expression correlates with NRGN and CALB1 in healthy subjects and AD patients. Cells. 2021;10:18. https://doi.org/10.3390/cells10040882.
5. Patterson VL, Zullo AJ, Koenig C, Stoessel S, Jo H, Liu XR, et al. Neural-specific deletion of Htra2 causes cerebellar neurodegeneration and defective processing of mitochondrial OPA1. PLoS One. 2014;9:24. https://doi.org/10.1371/journal.pone.0115789.
6. Del Pilar C, Lebrón-Galán R, Pérez-Martín E, Pérez-Revuelta L, Ávila-Zarza CA, Alonso JR, et al. The selective loss of Purkinje cells induces specific peripheral immune alterations. Front Cell Neurosci. 2021;15:773696. https://doi.org/10.3389/fncel.2021.773696.
7. Kolinko Y, Krakorova K, Cendelin J, Tonar Z, Kralickova M. Microcirculation of the brain: morphological assessment in degenerative diseases and restoration processes. Rev Neurosci. 2015;26:75–93. https://doi.org/10.1515/revneuro-2014-0049.
8. Skaaraas G, Melbye C, Puchades MA, Leung DSY, Jacobsen O, Rao SB, et al. Cerebral amyloid angiopathy in a mouse model of Alzheimer's disease associates with upregulated angiopoietin and downregulated hypoxia-inducible factor. J Alzheimers Dis. 2021;83:1651–63. https://doi.org/10.3233/jad-210571.
9. Fernandez-Klett F, Brandt L, Fernandez-Zapata C, Abuelnor B, Middeldorp J, Sluijs JA, et al. Denser brain capillary network with preserved pericytes in Alzheimer's disease. Brain Pathol. 2020;30:1071–86. https://doi.org/10.1111/bpa.12897.
10. Roitbak T, Li L, Cunningham LA. Neural stem/progenitor cells promote endothelial cell morphogenesis and protect endothelial cells against ischemia via HIF-1 alpha-regulated VEGF signaling. J Cereb Blood Flow Metab. 2008;28:1530–42. https://doi.org/10.1038/jcbfm.2008.38.
11. Mitoma H, Manto M, Gandini J. Recent advances in the treatment of cerebellar disorders. Brain Sci. 2019;10. https://doi.org/10.3390/brainsci10010011.
12. Cendelin J. From mice to men: lessons from mutant ataxic mice. Cerebellum Ataxias. 2014;1:4. https://doi.org/10.1186/2053-8871-1-4.
13. Cendelin J, Cvetanovic M, Gandelman M, Hirai H, Orr HT, Pulst SM, et al. Consensus paper: strengths and weaknesses of animal models of spinocerebellar ataxias and their clinical implications. Cerebellum. 2022;21:452–81. https://doi.org/10.1007/s12311-021-01311-1.
14. Kolinko Y, Cendelin J, Kralickova M, Tonar Z. Smaller absolute quantities but greater relative densities of microvessels are associated with cerebellar degeneration in lurcher mice. Front Neuroanat. 2016;10:35. https://doi.org/10.3389/fnana.2016.00035.
15. Babuska V, Houdek Z, Tuma J, Purkartova Z, Tumova J, Kralickova M, et al. Transplantation of embryonic cerebellar grafts improves gait parameters in ataxic lurcher mice. Cerebellum. 2015;14:632–41. https://doi.org/10.1007/s12311-015-0656-x.
16. Cendelin J, Purkartova Z, Kubik J, Ulbricht E, Tichanek F, Kolinko Y. Long-term development of embryonic cerebellar grafts in two strains of lurcher mice. Cerebellum. 2018;17:428–37. https://doi.org/10.1007/s12311-018-0928-3.
17. Purkartova Z, Tichanek F, Kolinko Y, Cendelin J. Embryonic cerebellar graft morphology differs in two mouse models of cerebellar degeneration. Cerebellum. 2019;18:855–65. https://doi.org/10.1007/s12311-019-01067-9.
18. Fernandez-Gonzalez A, La Spada AR, Treadaway J, Higdon JC, Harris BS, Sidman RL, et al. Purkinje cell degeneration (pcd) phenotypes caused by mutations in the axotomy-induced gene, Nna1. Science. 2002;295:1904–6. https://doi.org/10.1126/science.1068912.
19. Kyuhou S, Kato N, Gemba H. Emergence of endoplasmic reticulum stress and activated microglia in Purkinje cell degeneration mice. Neurosci Lett. 2006;396:91–6. https://doi.org/10.1016/j.neulet.2005.11.023.
20. Chakrabarti L, Eng J, Ivanov N, Garden GA, La Spada AR. Autophagy activation and enhanced mitophagy characterize the Purkinje cells of pcd mice prior to neuronal death. Mol Brain. 2009;2:24. https://doi.org/10.1186/1756-6606-2-24.
21. Baltanas FC, Berciano MT, Valero J, Gomez C, Diaz D, Alonso JR, et al. Differential glial activation during the degeneration of Purkinje cells and mitral cells in the PCD mutant mice. Glia. 2013;61:254–72. https://doi.org/10.1002/glia.22431.
22. Mullen RJ, Eicher EM, Sidman RL. Purkinje cell degeneration, a new neurological mutation in the mouse. Proc Natl Acad Sci U S A. 1976;73:208–12.
23. Ghetti B, Norton J, Triarhou LC. Nerve cell atrophy and loss in the inferior olivary complex of "Purkinje cell degeneration" mutant mice. J Comp Neurol. 1987;260:409–22. https://doi.org/10.1002/cne.902600307.
24. Triarhou LC. Biological clues on neuronal degeneration based on theoretical fits of decay patterns: towards a mathematical neuropathology. Folia Neuropathol. 2010;48:3–10.
25. Triarhou LC, Norton J, Ghetti B. Anterograde transsynaptic degeneration in the deep cerebellar nuclei of Purkinje cell degeneration (pcd) mutant mice. Exp Brain Res. 1987;66:577–88.
26. Blanks JC, Mullen RJ, LaVail MM. Retinal degeneration in the pcd cerebellar mutant mouse. II. Electron microscopic analysis. J Comp Neurol. 1982;212:231–46. https://doi.org/10.1002/cne.902120303.
27. LaVail MM, Blanks JC, Mullen RJ. Retinal degeneration in the pcd cerebellar mutant mouse .I. Light microscopic and autoradiographic analysis. J Comp Neurol. 1982;212:217–30. https://doi.org/10.1002/cne.902120302.
28. Blanks JC, Spee C. Retinal degeneration in the pcd/pcd mutant mouse: accumulation of spherules in the interphotoreceptor space. Exp Eye Res. 1992;54:637–44.
29. O'Gorman S, Sidman RL. Degeneration of thalamic neurons in "Purkinje cell degeneration" mutant mice. I. Distribution of neuron loss. J Comp Neurol. 1985;234:277–97. https://doi.org/10.1002/cne.902340302.
30. Kolinko Y, Marsalova L, Pena SP, Kralickova M, Mouton PR. Stereological changes in microvascular parameters in hippocampus of a transgenic rat model of Alzheimer's disease. J Alzheimers Dis. 2021;84:249–60. https://doi.org/10.3233/jad-210738.
31. Kleiter N, Lametschwandtner A. Microvascularization of the cerebellum in the turtle, Pseudemys scripta elegans (Reptilia). A scanning electron microscope study of microvascular corrosion casts, including stereological measurements. Anat Embryol (Berl). 1995;191:145–53.
32. Mouton PR. Principles and practices of unbiased stereology: an introduction for bioscientists. Baltimore, Maryland, USA: Johns Hopkins University Press; 2002.
33. Mouton PR. Unbiased stereology: a concise guide. Baltimore, Maryland, USA: Johns Hopkins University Press; 2011.
34. Sterio DC. The unbiased estimation of number and sizes of arbitrary particles using the disector. J Microsc. 1984;134:127–36. https://doi.org/10.1111/j.1365-2818.1984.tb02501.x.
35. Nyengaard JR, Marcussen N. The number of glomerular capillaries estimated by an unbiased and efficient stereological method. J Microsc. 1993;171:27–37. https://doi.org/10.1111/j.1365-2818.1993.tb03356.x.
36. Lee GD, Aruna JH, Barrett PM, Lei DL, Ingram DK, Mouton PR. Stereological analysis of microvascular parameters in a double transgenic model of Alzheimer's disease. Brain Res Bull. 2005;65:317–22. https://doi.org/10.1016/j.brainresbull.2004.11.024.
37. West MJ. Space balls revisited: stereological estimates of length with virtual isotropic surface probes. Front Neuroanat. 2018;12:49. https://doi.org/10.3389/fnana.2018.00049.

38. Isaacs KR, Anderson BJ, Alcantara AA, Black JE, Greenough WT. Exercise and the brain: angiogenesis in the adult rat cerebellum after vigorous physical activity and motor skill learning. J Cereb Blood Flow Metab. 1992;12:110–9. https://doi.org/10.1038/jcbfm.1992.14.
39. Gundersen HJ, Jensen EB, Kieu K, Nielsen J. The efficiency of systematic sampling in stereology–reconsidered. J Microsc. 1999;193:199–211.
40. Wang TY, Morgan JI. The Purkinje cell degeneration (pcd) mouse: an unexpected molecular link between neuronal degeneration and regeneration. Brain Res. 2007;1140:26–40. https://doi.org/10.1016/j.brainres.2006.07.065.
41. Rhyu IJ, Bytheway JA, Kohler SJ, Lange H, Lee KJ, Boklewski J, et al. Effects of aerobic exercise training on cognitive function and cortical vascularity in monkeys. Neuroscience. 2010;167:1239–48. https://doi.org/10.1016/j.neuroscience.2010.03.003.
42. Swain RA, Harris AB, Wiener EC, Dutka MV, Morris HD, Theien BE, et al. Prolonged exercise induces angiogenesis and increases cerebral blood volume in primary motor cortex of the rat. Neuroscience. 2003;117:1037–46. https://doi.org/10.1016/s0306-4522(02)00664-4.
43. Caddy KW, Biscoe TJ. Structural and quantitative studies on the normal C3H and Lurcher mutant mouse. Philos Trans R Soc Lond B Biol Sci. 1979;287:167–201.
44. Vernet-der Garabedian B, Lemaigre-Dubreuil Y, Delhaye-Bouchaud N, Mariani J. Abnormal IL-1beta cytokine expression in the cerebellum of the ataxic mutant mice staggerer and lurcher. Brain Res Mol Brain Res. 1998;62:224–7.